HHS Public Access

Author manuscript

Nanomedicine. Author manuscript; available in PMC 2018 July 01.

Published in final edited form as:

Nanomedicine. 2017 July ; 13(5): 1693–1701. doi:10.1016/j.nano.2017.03.005.

EVALUATION OF ANTITUMOR ACTIVITY AND CARDIAC TOXICITY OF A BONE-TARGETED pH-SENSITIVE LIPOSOMAL FORMULATION IN A BONE METASTASIS TUMOR MODEL IN MICE

Diego dos Santos Ferreira[a,b], **Bruno Luís Jesus de Oliveira Pinto**[a], **Vidhya Kumar**[a], **Valbert Nascimento Cardoso**[c], **Simone Odília Fernandes**[c], **Cristina Maria Souza**[d], **Geovanni Dantas Cassali**[d], **Anna Moore**[a], **David Sosnovik**[a], **Christian Farrar**[a], **Elaine Amaral Leite**[b], **Ricardo José Alves**[b], **Mônica Cristina de Oliveira**[b], **Alexander Ramos Guimarães**[e], and **Peter Caravan**[a]

[a]Athinoula A. Martinos Center for Biomedical Imaging, Massachusetts General Hospital, Harvard Medical School, 149 13th St, Charlestown, MA 02129, USA

[b]Department of Pharmaceutical Products, Faculty of Pharmacy, Universidade Federal de Minas Gerais, Av. Pres. Antônio Carlos, 6627, Pampulha, Belo Horizonte, MG 31270-901, Brazil

[c]Department of Clinical and Toxicology Analyses, Faculty of Pharmacy, Universidade Federal de Minas Gerais, Av. Pres. Antônio Carlos, 6627, Pampulha, Belo Horizonte, MG 31270-901, Brazil

[d]Department of Pathology, Institute of Biological Sciences, Universidade Federal de Minas Gerais, Av. Pres. Antônio Carlos, 6627, Pampulha, Belo Horizonte, MG 31270-901, Brazil

[e]Department of Diagnostic Radiology, Oregon Health & Sciences University, 3181 SW Sam Jackson Park Rd, Portland, OR 97239, USA

Abstract

Chemotherapy for bone tumors is a major challenge because of the inability of therapeutics to penetrate dense bone mineral. We hypothesize that a nanostructured formulation with high affinity for bone could deliver drug to the tumor while minimizing off-target toxicity. Here, we evaluated the efficacy and toxicity of a novel bone-targeted, pH-sensitive liposomal formulation containing doxorubicin in an animal model of bone metastasis. Biodistribution studies with the liposome showed good uptake in tumor, but low accumulation of doxorubicin in the heart. Mice treated with the bone-targeted liposome formulation showed a 70% reduction in tumor volume, compared to

Corresponding author: Peter Caravan, caravan@nmr.mgh.harvard.edu, Phone: 1-617-643-0193, Building 149, Room 2301, 13th Street, Charlestown, MA 02129 USA.

Conflict of interest: The authors declare no commercial associations, current and within the past five years, that might pose a potential, perceived or real conflict of interest with this work.

Previous presentation of abstract: Part of this work was presented at the 2016 Controlled Release Society Annual Meeting, Seattle, WA, USA.

35% reduction for free doxorubicin at the same dose. Both cardiac toxicity and overall mortality were significantly lower for animals treated with the bone-targeted liposomes compared to free drug. Bone-targeted, pH-sensitive, doxorubicin containing liposomes represent a promising approach to selectively delivering doxorubicin to bone tumors while minimizing cardiac toxicity.

Graphical abstract

Bone-targeted alendronate-coated liposomes containing doxorubicin (SpHL-AL-DOX) provide increased uptake in bone metastases, higher antitumor activity, reduced cardiac toxicity and reduced mortality rate when compared to either free doxorubicin or untargeted liposomes.

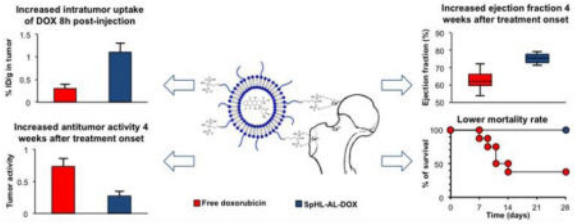

Keywords

hydroxyapatite-targeting; bisphosphonates; doxorubicin; bone tumor; cardiotoxicity

INTRODUCTION

Many advanced cancers metastasize to the bone, e.g. 60 to 75% of breast metastases occur in bones [1]. These metastatic foci are characterized by increased osteoclastic activity and osteolysis, and are associated with pain, fractures, and nerve compression syndromes. The end result is decreased quality of life [2]. There has been little improvement in drug development in patients with metastatic breast cancer to the skeleton. In this context, effective therapies to inhibit the progression of bone metastases would have important clinical benefits.

Liposomal formulations have become well established to deliver chemotherapies. To further improve drug delivery to tumors, pH-sensitive liposomes have been developed. These liposomes are designed to be less stable in an acidic environment as occurs in the tumor extracellular matrix as well as within endosomes [3]. Further selectivity may be achieved by active targeting of the liposome to the tumor site.

A major characteristic of bone is its high content of the mineral hydroxyapatite (HA). HA limits the diffusion of drugs into the bone and prevents access to less vascularized areas [4]. Among drugs shown to accumulate in bones, the bisphosphonates have been studied as targeting vectors, either by direct conjugation to non-specific bone therapeutic agents or by conjugation to the surface of drug delivery systems such as liposomes [5–10]. Bisphosphonates have been shown to target bone tumors, likely due to the increased vascularity associated with the tumor and because of osteoclast activity surrounding the tumor which results in increased HA surface area [11]. In a previous work from our group,

we developed a pH-sensitive, bone-targeted liposomal formulation containing the anticancer drug doxorubicin (DOX) and proved its ability of interacting with the bone matrix and release the drug under reduced pH environments [12]. From our knowledge, this was the first liposomal formulation to successfully combine pH-sensitivity with bisphosphonate conjugation to actively target bone tumors.

In the current work these alendronate-coated pH-sensitive liposomes containing DOX (SpHL-DOX) were prepared, evaluated in a mouse model of metastatic breast cancer to the bone, and compared to untargeted liposomes or free DOX. Single photon emission computed tomography (SPECT) and bioluminescence imaging (BLI) were used to characterize the animal model and to monitor treatment response. We studied the effect of the different formulations on survival, tumor size, and cardiotoxicity.

METHODS

Material

Cholesteryl hemisuccinate (CHEMS), doxorubicin, 4-(2-hydroxyethyl)-1-piperazineethanesulfonic acid (HEPES) sodium salt, sodium alendronate, sodium hydroxide, and D-luciferin were obtained from Sigma Chemical Company (Saint Louis, MI, USA). Lipoid GmbH (Ludwigshafen, Germany) supplied Dioleoylphosphatidylethanolamine (DOPE) and 1,2-distearoyl-sn-glycero-3-phosphoethanolamine-N-(polyethyleneglycol-2000) (DSPE-PEG2000). Dulbecco's modified Eagle's medium (DMEM) was purchased from Gibco (Grand Island, NY, USA). The human breast adenocarcinoma cell line (MDA-MB-231) was purchased from American Type Culture Collection (Manassas, VA, USA). Xylazine solution (Dopaser™ 2%) was obtained from Hertape Calier (Juatuba, MG, Brazil). Ketamine hydrochloride solution (Dopalen™ 10%) was purchased from Vetbrands Agroline (Campo Grande, MT, Brazil). HYNIC-βAla-Bombesin$_{7–14}$(^{99m}Tc-BBN$_{7–14}$) peptide was supplied by GL BioChem (Shanghai Shi, China), and technetium-99m was obtained by a molybdenum-99/technetium-99m generator from Instituto de Pesquisas Energéticas (São Paulo, Brazil). All other chemicals used in this study were of analytical grade.

Liposome preparation

Alendronate-coated pH-sensitive liposomes containing DOX (SpHL-AL-DOX) composed by DOPE, CHEMS, and DSPE-PEG$_{3400}$-AL (5.7:3.8:0.5 molar ratio and DOX at 2 mg•mL^{-1}) as well as alendronate-non coated pH-sensitive liposomes containing DOX (SpHL-DOX), composed by DOPE, CHEMS, DSPE-PEG$_{2000}$ (5.7:3.8:0.5 molar ratio and DOX at 2 mg•mL^{-1}) were prepared by thin film hydration method followed by extrusion and DOX encapsulation by remote loading driven by a transmembrane sulphate gradient, as previously described [12]. Details about the preparation and physicochemical characterization are described in the Supplementary Information.

Tumor model

All animal experiments were performed according to the experimental guidelines of the Animal Experimentation Ethics Committee of Universidade Federal de Minas Gerais and

the Massachusetts General Hospital Subcommittee on Research Animal Care. Female nude Balb/C mice bearing MDA-MB-231 bone metastasis were employed in this study. Tumor bearing mice were established as following: 10^5 MDA-MB-231 cells were inoculated into the medullar channel of the left tibia of mice. Tumors were allowed to grow for 15 days and ^{99m}Tc-methylene diphosphonate (MDP) SPECT, ^{99m}Tc-BBN$_{7–14}$ SPECT, and BLI were used to confirm the presence of the tumor. After image acquisition, animals were euthanized and the legs were collected for histological analyses. Formalin-fixed samples were dehydrated gradually in ethanol, embedded in paraffin, cut into 4-mm sections, stained with hematoxylin-eosin and examined under light microscopy.

SPECT images

Aliquots of 3.7 MBq of ^{99m}Tc-BBN$_{7–14}$ or ^{99m}Tc-MDP were injected intravenously into tumor-bearing mice (n = 3). After 1 hour, mice were anesthetized with a mixture of xylazine (8 mg•kg^{-1}) and ketamine (80 mg•kg^{-1}), and then placed horizontally under the collimator of a gamma camera (Mediso Medical Imaging System, Budapest, Hungary) employing a low-energy high-resolution collimator. Images were acquired using a 256 x 256 x 16 matrix size with a 20% energy window set at 140 KeV for a period of 300 s.

In vivo BLI images

In vivo imaging of bioluminescence for the evaluation of the tumor burden was performed by the *in vivo* imaging system IVIS (PerkinElmer, Waltham, MA, USA) on tumor-bearing mice (n = 3). After general anesthesia with 1.5% isoflurane in 50/50 O_2/medical air mixture with total flow rate of 1200 ml•min^{-1}, each mouse was intraperitoneally injected with D-Luciferin (150 mg•kg^{-1}). The acquisition time was defined by kinetics studies (Supplementary Information). Imaging was performed before and 12 minutes post-injection, using the following parameters: exposure time, 60 s; open emission filter; frame rate = 576 fps, f-number = 8 and field of view (FOV) = 13x13 cm. Tridimensional images were also acquired using the diffuse light imaging tomography technique in order to determine the exact position of the tumor (Supplementary Information).

Biodistribution studies

After 15 days of tumor growth, animals were intravenously injected with free DOX, SpHL-DOX or SpHL-AL-DOX (15 mg•kg^{-1}, n = 6 each group) and euthanized after 2 h (n = 3 per treatment) or 8 h (n = 3 per treatment). Blood, liver, spleen, kidney, heart, right and left tibias were collected for quantification of DOX by HPLC. Due to the low mass of tibia, the quantification of DOX in the healthy bone (right tibia) was not possible, falling below the detection limit. Blood was collected on heparinized tubes and centrifuged at 2000 × *g* for 10 min. To preserve DOX from degradation, all samples were stored at 20 °C until analysis. Methodological details about the quantification are described in Supplementary Information.

Antitumor activity and toxicity evaluation

Starting 15 days after the implantation of tumor cells, mice were intravenously injected with free DOX, SpHL-DOX or SpHL-AL-DOX (10 mg DOX per kg body weight, n = 8 for each group). Mice were dosed weekly for four weeks. The tumor response to treatment was

monitored by BLI every two weeks. For the toxicity evaluation, healthy animals were divided in four groups and intravenously injected with a 10 mg•kg^{-1} DOX dose of either free DOX, SpHL-DOX or SpHL-AL-DOX (n = 8 per group), or injected with NaCl 0.9% (w•v-1) vehicle solution (n = 5 for this group). Animals were dosed weekly for up to four weeks. Toxicity was monitored by CINE cardiac MRI images analysis. Kaplan-Meyer survival curves were computed and compared by Mantel-Cox analyses. Parameters of median survival, p-value and death risk ratio were calculated based on these survival curves.

CINE cardiac MRI

Cardiac magnetic resonance imaging (MRI) was performed on a 9.4-tesla MRI scanner (Bruker Biospin, Billerica, MA, USA) with a custom-built transmit-receive surface coil (elliptical shaped coil with major axis radius of 20 mm and minor axis radius of 15 mm) placed over the anterior chest wall. Mice were positioned supine on a custom made mouse cradle and anesthetized with 1.5% isoflurane in 50/50 O_2/medical air mixture with total flow rate of 1200 ml•min^{-1}. A physiological monitoring system (SA Instruments Inc., Stony Brook, NY, USA) was used to monitor the ECG, respiration and body temperature. Ungated triplanar localizer images were acquired using a fast imaging with steady-state precession (FISP) sequence. FISP image acquisition parameters consisted of TE/TR = 1.05/2.1 ms, 128 segments, scan TR = 8.17 ms, FA = 60°, NA = 1, FOV = 40x40 mm, matrix = 128x128, slice thickness = 1 mm, 3 orthogonal slices. Next an ECG gated FISP sequence was used to acquire short and long axis views of the left ventricle. Image acquisition parameters consisted of TE/TR = 0.96/2.832 ms, 32 segments, scan TR = 19.18 ms, FA = 30°, NA = 4, FOV = 25x25 mm, matrix = 128x128, slice thickness = 1 mm, and 5 image slices. The gated FISP images were then used to prescribe a series of ECG and respiratory gated short axis fast low-angle shot (FLASH) CINE images that were acquired throughout the heart. FLASH CINE acquisition parameters consisted of TE/TR=1.09/4.275 ms, FLASH TR = 10.9 ms, 20 images/RR interval, FA=25°, NA=4, FOV=25x25 mm, matrix=160x160.

The epicardial and endocardial borders were outlined in end diastolic and end systolic frames using the free hand drawing function of ImageJ (Scion Corporation, Frederick, MD, USA). All analyses were performed by the same reader (D.S.F). The number of voxels in each compartment multiplied by the voxel size of 0.015 mm^3 yielded the respective volumes. Global end diastolic volume (EDV), end systolic volume (ESV), stroke volume (SV = EDV – ESV), and ejection fraction (EF = SV/EDVx100) were calculated. The endocardial diameter (ED) was also outlined in the medial slice at the end of diastole (DED) and systole (SED) to determine the absolute fractional shortening (aFS = DED – SED) and relative FS (FS = aFS/DEDx100).

RESULTS

Liposome preparation

The physicochemical characteristics of SpHL-AL-DOX and SpHL-DOX are summarized in Table 1. The average diameter was close to 150 nm for both formulations. The low polidispersity index (PdI) vales are consistent with the presence of homogeneously dispersed formulations. The zeta potential of the SpHL-AL-DOX formulation was slightly more

negative than for SpHL-DOX. Similarly, the encapsulation efficacy was also increased for SpHL-AL-DOX.

Characterization of the tumor model

Fifteen days post-tumor cell injection into the medullary cavity of the tibia of Balb-c nu/nu female mice, animals were imaged using ^{99m}Tc-MDP SPECT, ^{99m}Tc-BBN$_{7–14}$ SPECT and BLI. ^{99m}Tc-MDP is a bone-seeking radiopharmaceutical that is used clinically to detect metastases to the bone. ^{99m}Tc-BBN$_{7–14}$ is a bombesin derivative that targets the gastrin releasing peptide (GRP) receptor expressed on many cancer cells including the MDA-MB-231 cell line used here [13,14]. We also used a variant of the MDA-MB-231 cell line that expresses luciferase. These cells could be directly imaged using bioluminescence after administration of D-luciferin.

Figures 1A and 1B show scintigraphic images of a control and a tumor-bearing mouse, respectively, acquired one hour after injection of ^{99m}Tc-MDP. The control mouse was injected with a saline solution into the medullary cavity 15 days prior to imaging. There is clearly a region of high tracer uptake in the tumor-bearing animal (arrow). Region of interest analysis on the ipsilateral (tumor or saline injection site) and contralateral thigh, revealed an ipsi:contralateral ratio of 0.9 ± 0.2 for the control animals, which is consistent with the absence of preferential accumulation of the ^{99m}Tc-MDP into the injection site and indicates that there is no active inflammation process in the region. On the other hand the ipsi:contralateral ratio in the tumor bearing mice was 1.5 ± 0.3. The GRP receptor-targeting ^{99m}Tc-BBN$_{7–14}$ probe also clearly delineated the tumor (Figure 1C) and localized it to the joint. The ipsi:contralateral ratio for ^{99m}Tc-BBN$_{7–14}$ was 2.1 ± 0.5.

Presence of tumor was also confirmed by BLI with images acquired 12 minutes post-injection of D-luciferin. The most intense signal was in the proximal region of the tibia (Figure 1D–F). Also, tumor spread is observed toward the distal region of the tibia. After the SPECT and BLI acquisitions, the animals were euthanized and the legs were collected for histological analyses. Analyzing the proximal head of tumor-bearing tibia (Figure 1G, 1H) neoplastic cells were observed to be arranged predominantly in a solid pattern, forming large, slightly basophilic areas. The tumor growth was accompanied by reduction of trabecular and spongeous bone, in consequence to the activation of bone turnover processes. Histology also showed invasion of the tumor into the periosteal region and adjacent muscle.

Biodistribution studies

We next performed some biodistribution studies of the three formulations of DOX in the tumor model to determine whether there was preferential uptake of the targeted liposomal formulation. DOX content was quantified in each organ and calculated as %ID•g^{-1} of tissue (Table 2). For the free DOX group, we observed a large uptake of DOX in the kidneys at 2 h post-injection, while after 8 h the DOX level in the kidneys is reduced by a factor of six. The reduction of kidney uptake is mirrored by complete elimination of DOX from the bloodstream. It should be noted also that the uptake of free DOX into heart and tumor tissues at 2 h was four times higher when compared to blood. Other organs showed a relatively lower drug uptake at both time points.

For the liposomal DOX, both formulations showed significant uptake by liver and spleen. High renal excretion was also suggested by the decrease in kidney uptake with time. Other organs evaluated showed significantly lower DOX uptake at both time points. The heart uptake of DOX is significantly reduced (P = 0.028) for SpHL-AL-DOX at 2h-post injection when compared to free drug. For SpHL-DOX, the average uptake of DOX in the heart was reduced two-fold when compared to free DOX, but this result did not reach statistical significance in the small sample size (P = 0.083, n = 3). At 8h-post injection the heart uptake of both liposomal DOX formulations approaches zero. The liposomal formulations resulted in higher blood concentrations compared to free DOX at 2 hours, In parallel, the uptake in tumor area at 2 hours is increased for the SpHL-AL-DOX treatment relative to free DOX. DOX was also retained in the tumor area for a longer period of time for the SpHL-AL-DOX treatment group when compared to the others. The DOX concentration in the tumor area 8 h post injection for the SpHL-AL-DOX-treated group was four times higher than for free DOX and two times higher than for SpHL-DOX

Antitumor activity

On the basis of the positive biodistribution results, we next investigated whether the liposomal formulations would be effective for reducing tumor growth in vivo. Animals were divided into 4 groups and treated weekly with free DOX, SpHL-DOX, SpHL-AL-DOX, or vehicle at a constant DOX doses of 10 mg•kg^{-1}. Tumor growth was quantified by BLI every two weeks. Tumor volume was quantified by measuring the photon radiance (photon per second per square centimeter per steradian) within a region of interest (ROI) drawn around the tumor area. The ROIs were the same size for all animals at all time points. The results were plotted as percentage of change in photon radiance compared to the images before treatment began.

For the animals treated with both free and liposomal DOX, a reduction of tumor volume was observed when compared to the vehicle-treated group. For the vehicle-treated control group, the photon radiance increased from 6 times baseline at day 14 to 150 times at day 28, indicating substantial tumor proliferation. The animals treated with the different DOX formulations all showed a reduction in tumor volume over time. The most effective formulation was SpHL-AL-DOX, which reduced tumor volume by 70% compared to baseline. For free DOX, the reduction of photon radiance at day 28 was 35% of the baseline image. SpHL-DOX presented an intermediate result.

Cardiotoxicity Evaluation

Given the favorable biodistribution profiles of both liposomal formulations with respect to heart uptake, we anticipated that the cardiotoxicity of the liposomal formulations would be lower than with free DOX. We used MRI to assess cardiac function in mice treated with the three different DOX formulations and compared the cardiac function in these mice to that of vehicle-treated mice. Mice were treated with a DOX formulation at a dose of 10•mg kg^{-1} or with saline vehicle weekly for 4 weeks. Mice were imaged with cardiac MRI one week after the last dose administration. After cardiac MRI, EDV, ejection fraction and fractional shortening were determined for each animal and the results are represented in Figure 3.

Vehicle-treated mice had an EDV of 8.5 ± 2.1 mm^3, an ejection fraction of 75.8 ± 3.1 % and fractional shortening of 59.4 ± 2.8 %. Only 3 mice treated with free DOX survived out to the imaging time point. Those mice had similar EDV (8.2 ± 1.6 mm^3, P = 0.734) significantly lower ejection fraction (62.0 ± 5.5 %, P = 0.0035) and fractional shortening (44.2 ± 4.2, P = 0.0008) compared to the vehicle treated group. On the other hand, mice treated with either liposomal formulation (SpHL-DOX or SpHL-AL-DOX) showed similar EDV (9.1 ± 2.2 mm^3, P = 0.641 for SpHL-DOX, 7.9 ± 2.3 mm^3, P = 0.543 for SpHL-AL-DOX), and ejection fractions (73.8 ± 4.8 %, P = 0.4564 for SpHL-DOX, 74.1 ± 4.7 %, P = 0.4914 for SpHL-AL-DOX) to the vehicle-treated control group. There was a small, but significant reduction in fractional shortening for both liposomal formulations compared to the control animals (53.1 ± 3.6 %, P = 0.015 for SpHL-DOX and 54.1 ± 3.9 % for SpHL-AL-DOX, P = 0.024). Nonetheless, it was possible to observe a protection against the cardiotoxicity for these groups when compared to animals treated with free-DOX.

Evaluation of mortality rate

We next evaluated the effect of the different DOX formulations on mortality in healthy or tumor-bearing animals. We observed a higher mortality rate for animals treated with free DOX when compared to animals treated with either SpHL-DOX or SpHL-AL-DOX for both healthy and tumor-bearing animals (Figure 4). The median survival, death risk ratio and p-values compared to the control group or to the SpHL-AL-DOX treated animals are presented in Table 4. For healthy animals, there is a higher mortality rate for DOX, with a strong and significant reduction in median survival and increased death risk ratio when compared to both the SpHL-AL-DOX-treated animals and the control group. In the tumor-bearing animals, we observed a similar mortality rate for free DOX and control animals, and both are higher than the liposome-treated animals (SpHL-DOX or SpHL-AL-DOX).

On the other hand, the tumor-bearing animals treated with either SpHL-AL-DOX or SpHL-DOX both showed a reduction in mortality rate when compared to both free DOX and the control groups. For the healthy animals, again we observed a strongly reduced mortality rate for the SpHL-AL-DOX treatment group when compared to the free DOX group with the death risk ratio 11 times lower in the SpHL-AL-DOX treatment group. The mortality rate was similar for the SpHL-AL-DOX treatment and the control groups. Comparing the two liposomal formulations, we observed a 9-fold higher death risk for the SpHL-DOX treatment group in healthy animals compared to the SpHL-AL-DOX treatment group.

DISCUSSION

Both of the formulations developed in this work presented suitable physicochemical characteristics for application in *in vivo* efficacy and toxicity studies. The average diameter below 200 nm for both formulations has been shown to be suitable to increase tumor uptake, while reducing DOX accumulation in healthy organs [15]. The negative zeta potentials measured may result in increased physical stability of these formulations due to electrostatic repulsion, reducing the risk of aggregation. SpHL-AL-DOX exhibited a more negative zeta potential value, which could be related to the presence of the negatively charged phosphonate groups on the liposomal surface at neutral pH [16]. The high encapsulation

percentages allow application of a small intravenous volume of liposomal dispersion in order to achieve a therapeutic dose. The highest encapsulation percentage was achieved with SpHL-AL-DOX owing to the additional electrostatic interaction between the deprotonated phosphonate groups and positively charged DOX.

In order to proceed to animal studies, we have developed a MDA-MB-231 cell line bone-metastasis tumor model. The tumor-bearing animals were imaged by SPECT with the bone-seeking probe ^{99m}Tc-MDP and the tumor-seeking probe ^{99m}Tc-BBN$_{7–14}$. As expected both probes were able to identify the tumor with a higher ipsi:contralateral ratio for the ^{99m}Tc-BBN$_{7–14}$ images. The larger effect observed with ^{99m}Tc-BBN$_{7–14}$ may be explained by spreading of the tumor to the muscle adjacent to the tumor cell inoculation site. The growth pattern of the tumor observed in this model is in agreement with that previously described in literature [17]. These results were further confirmed by BLI which showed a higher accumulation of the tumor in the areas composed mainly by spongeous bone, which is more accessible for tumor cells to spread, associated to dissemination of tumor cells into the medullary channel of the bone [18].

By biodistribution analyses, we have shown the rapid elimination of free DOX from the bloodstream. Recent studies using this drug in a mammary tumor model in Balb C mice showed a biphasic plasma half-life with α half-life of 4.5 min and a β half-life of 277.2 min [19]. This pharmacokinetic behavior is consistent with our observed low concentration of DOX in blood 2h-post injection and the negligible concentration after 8 hours. On the other hand, the liposomes presented a longer circulation time and higher uptake in liver and spleen [20]. Higher tumor uptake and reduced heart uptake was seen for the liposomal formulations when compared to the free drug. These differences can be explained by two factors: (1) because of the size of the liposomes, the DOX is less susceptible to uptake in healthy tissues, such as myocardium; (2) encapsulation of DOX in long-circulating liposomes allow for this drug to be retained for a long time in the bloodstream, enhancing its capacity of reaching the tumor area and being taken up by the EPR effect [21]. Also, the higher tumor uptake for SpHL-AL-DOX compared to SpHL-DOX can be explained by the presence of alendronate on the liposomal surface, which allows for the interaction of this formulation with the local bone matrix, with increased release of DOX in that area [22].

In antitumor activity studies the SpHL-AL-DOX formulation was more efficient for inhibition of tumor growth than free DOX, while the SpHL-DOX presented an intermediate result between the other two groups. These results indicate that both drug delivery modifications, pH-sensitive liposome encapsulation and liposomal surface modification with the alendronate bone-targeting vector, are important to achieve a higher antitumor activity.

A well-known limitation of DOX chemotherapy is cardiotoxicity. The mechanism for DOX-induced cardiotoxicity is controversial, and several hypotheses have been proposed [23]. It has been suggested that DOX induces an iron-mediated increase in reactive oxygen species [24,25] that is especially damaging to mitochondria, which are present at high concentration in areas with metabolic activity, such as the cardiac tissue [26,27]. Another hypothesis centers on the capacity of DOX to interact with cardiolipin, an important phospholipid related to electron-transport in the myocardium, reducing its activity and subsequently

damaging the myocardium [27,28]. Both mechanisms would lead to the reduction of the heart contractility. In our cardiotoxicity study we have proved this loss of contractility after DOX treatment, consistent with results previously reported [29]. In contrast, for the liposomal formulations, the cardiac parameters remained constant after the treatment, proving the protective effect caused by the liposomal encapsulation of this drug.

The DOX toxicity was also reflected in a higher mortality rate for both healthy and tumor-bearing animals. For the healthy animals, the higher mortality rate for free DOX can be ascribed to its cardiotoxicity, as observed in the CINE cardiac MRI studies, as well as the established renal toxicity of DOX [30], while for the tumor-bearing the higher mortality for the free drug could be associated to two factors: (1) the high cardio- and renal toxicity of DOX and (2) the inability of free DOX to completely suppress tumor growth. On the other hand, the SpHL-AL-DOX group presented the lowest risk of mortality in both situations. The improved survival can be explained by the increased antitumor activity of SpHL-AL-DOX, which could reduce the death risk as a consequence of the cancer, and also by the reduced cardiotoxicity as evidenced by the cardiac MRI studies. The intermediate performance for SpHL-DOX may be related to its lower plasma stability, possibly due to interaction with plasma proteins followed by DOX release, as shown in previous studies from our group [12].

This work demonstrates that encapsulation of DOX in pH-sensitive liposomes can reduce the toxic effects of this drug, leading to a longer life expectancy for bone tumor-bearing animals. Addition of the bone-targeting ligand alendronate to the surface of these liposomes further increased the specificity of this drug for the tumor, allowing for increased antitumor efficacy. This higher specificity contributed to a lower cardiotoxicity resulting in increased survival and a higher therapeutic index compared to free DOX. The SpHL-AL-DOX formulation is a potential therapy for the treatment of bone tumors especially bone metastases.

Supplementary Material

Refer to Web version on PubMed Central for supplementary material.

Acknowledgments

Funding: This work was supported by the National Institutes of Health [grant numbers R01EB009062, S10OD010650]; the Fundação de Amparo à Pesquisa do Estado de Minas Gerais, Belo Horizonte, Brazil [grant number REDE-40/11]; and Fundac a o Coordenac a o de Aperfeic oamento de Pessoal de Ni vel Superior [grant number: 6188-13-3].

Abbreviations

$BBN_{7–14}$	HYNIC-βAla-$Bombesin_{7–14}$
BLI	Bioluminescence Imaging
CHEMS	cholesteryl hemisuccinate
DMEM	Dulbecco's modified Eagle's medium
DOPE	Dioleoylphosphatidylethanolamine

DOX	doxorubicin
DSPE-PEG$_{2000}$	1,2-distearoyl-sn-glycero-3-phosphoethanolamine-N-(polyethyleneglycol-2000)
ED	endocardial diameter
EDV	end diastolic volume
EF	ejection fraction
ESV	end systolic volume
FISP	fast imaging with steady-state precession
FLASH	fast low-angle shot
FOV	field of view
GRP	gastrin releasing peptide
HA	hydroxyapatite
HEPES	4-(2-hydroxyethyl)-1-piperazineethanesulfonic acid
MDP	methylene diphosphonate
MRI	magnetic resonance imaging
PdI	polidispersity index
ROI	region of interest
SPECT	Single photon emission computed tomography
SpHL-AL-DOX	alendronate-coated pH-sensitive liposomes containing doxorubicin
SpHL-DOX	alendronate-non coated pH-sensitive liposomes containing doxorubicin
SV	stroke volume

References

1. Harvey H, Cream LR. Biology of bone metastases: Causes and consequences. Clin, Breast Cancer. 2007; 7:S7–S13. [PubMed: 17683652]
2. Mundy G. Metastasis to bone: causes, consequences and therapeutic opportunities. Nat Rev Cancer. 2002; 2:584–593. [PubMed: 12154351]
3. Ferreira DS, Lopes SCA, Franco MS, Oliveira MC. pH-sensitive liposomes for drug delivery in cancer treatment. Ther Deliv. 2013; 4:1099–1123. [PubMed: 24024511]
4. Shea J, Miller S. Skeletal function and structure: Implications for tissue-targeted therapeutics. Adv Drug Deliver Rev. 2005; 57:945–957.

5. Klenner T, Valenzuela-Paz P, Keppler B, Angres G, Scherf H, Wingen F, et al. Cisplatin-linked phosphonates in the treatment of the transplantable osteosarcoma in vitro and in vivo. Cancer Treat Rev. 1990; 17:253–259. [PubMed: 2272041]
6. Bauss F, Esswein A, Reiff K, Sponer G, Müller-Beckmann B. Effect of 17β-estradiol-bisphosphonate conjugates, potential bone-seeking estrogen pro-drugs, on 17β-estradiol serum kinetics and bone mass in rats. Calcif Tissue Int. 1996; 59:168–173. [PubMed: 8694893]
7. Lisic E, Phillips M, Ensor D, Nash K, Beets A, Knapp F. Synthesis of a new bisphosphonic acid ligand (SEDP) and preparation of a 188Re-(Sn)SEDP bone seeking radiotracer. Nucl Med Biol. 2001; 28:419–424. [PubMed: 11395315]
8. Anada T, Takeda Y, Honda Y, Sakurai K, Suzuki O. Synthesis of calcium phosphate- binding liposome for drug delivery. Bioorg Med Chem Lett. 2009; 19:4148–4150. [PubMed: 19523821]
9. Hengst V, Oussoren C, Kissel T, Storm G. Bone targeting potential of bisphosphonate-targeted liposomes: Preparation, characterization and hydroxyapatite binding in vitro. Int J Pharm. 2007; 331:224–227. [PubMed: 17150316]
10. Wang G, Mostafa N, Incani V, Kucharski C, Uludağ H. Bisphosphonate-decorated lipid nanoparticles designed as drug carriers for bone diseases. J Biomed Mater Res A. 2011; 100A: 684–693.
11. Smith MR. Osteoclast targeted therapy for prostate cancer: bisphosphonates and beyond. Urol Oncol. 2008; 24:420–425.
12. Ferreira DS, Faria SD, Lopes SCA, Teixeira CS, Malachias A, Magalhães-Paniago R, et al. Development of a bone-targeted pH-sensitive liposomal formulation containing doxorubicin: physicochemical characterization, cytotoxicity, and biodistribution evaluation in a mouse model of bone metastasis. Int J Nanomedicine. 2016; 9:3737–3751.
13. Dijkgraaf I, Boerman OC, Oyen WJ, Corstens FH, Gotthardt M. Development and application of peptide-based radiopharmaceuticals. Anticancer Agents Med Chem. 2007; 7:543–551. [PubMed: 17896914]
14. de Barros ALB, Mota LG, Soares DCF, de Souza CM, Cassali GD, Oliveira MC, et al. Long-circulating, pH-sensitive liposomes versus long-circulating, non-pH-sensitive liposomes as a delivery system for tumor identification. J Biomed Nanotechnol. 2013; 9:1636–1643. [PubMed: 23980511]
15. Torchilin VP. Targeted pharmaceutical nanocarriers for cancer therapy and imaging. AAPS J. 2007; 9:E128–E147. [PubMed: 17614355]
16. DeRuiter, J., Clark, R. Bisphosphonates: Calcium antiresorptive agents. 1. Spring; 2002.
17. Simmons JK, Hildreth BE, Supsavhad W, Elshafae SM, Hassan BB, Dirksen WP, et al. Animal Models of Bone Metastasis. Vet Pathol. 2015; 52:827–841. [PubMed: 26021553]
18. JiB, J. Di Fiore histologia. 1. Guanabara Koogan; 2003.
19. Fernandes RS, Silva JO, Lopes SCA, Chondrogiannis S, Rubello D, Cardoso VN, et al. Technetium-99m-labeled doxorubicin as an imaging probe for murine breast tumor (4T1 cell line) identification. Nucl Med Commun. 2016; 37:307–312. [PubMed: 26619397]
20. Carvalho-Junior A, Mota L, Nunan E, Wainstein A, Leal A, Cardoso VN, et al. Tissue distribution evaluation of stealth pH-sensitive liposomal cisplatin versus free cisplatin in Ehrlich tumor-bearing mice. Life Sciences. 2007; 80:659–664. [PubMed: 17141809]
21. Ulrich AS. Biophysical aspects of using liposomes as delivery vehicles. Bioscence Reports. 2002; 72:129–150.
22. Ferreira DS, Boratto FA, Cardoso VN, Serakides R, Fernandes SO, Ferreira LA, et al. Alendronate-coated long-circulating liposomes containing 99mtechnetium-ceftizoxime used to identify osteomyelitis. Int J Nanomedicine. 2015; 10:2441–2450. [PubMed: 25848262]
23. Simunek T, Sterba M, Popelova O, Adamcova M, Hrdina R, Gersl V. Anthracycline-induced cardiotoxicity: overview of studies examining the roles of oxidative stress and free cellular iron. Pharmacol Rep. 2009; 61:154–171. [PubMed: 19307704]
24. Berthiaume JM, Wallace KB. Adriamycin-induced oxidative mitochondrial cardiotoxicity. Cell Biol Toxicol. 2007; 23:15–25. [PubMed: 17009097]
25. Myers C. The role of iron in doxorubicin-induced cardiomyopathy. Seminars in oncology. 1998; 25:10–14.

26. Ichikawa Y, Ghanefar M, Bayeva M, Wu R, Khechaduri A, Naga Prasad SV, et al. Cardiotoxicity of doxorubicin is mediated through mitochondrial iron accumulation. J Clin Invest. 2014; 124:617–630. [PubMed: 24382354]

27. Goormaghtigh E, Huart P, Praet M, Brasseur R, Ruysschaert JM. Structure of the adriamycin-cardiolipin complex. Role in mitochondrial toxicity. Biophys Chem. 1990; 35:247–257. [PubMed: 2204444]

28. Schlame M, Rua D, Greenberg ML. The biosynthesis and functional role of cardiolipin. Prog Lipid Res. 2000; 39:257–288. [PubMed: 10799718]

29. Niu Q, Li Z, Du G, Qin X. 1H NMR based metabolomics profiling revealed doxorubicin- induced systematic alterations in rat model. J Pharm Biomed Anal. 2016; 118:338–348. [PubMed: 26595282]

30. Su Z, Ye J, Qin Z, Ding X. Protective effects of madecassoside against doxorubicin induced nephrotoxicity in vivo and in vitro. Sci Rep. 2015; 18314:1–14.

31. Alhareth K, Vauthier C, Gueutin C, Ponchel G, Moussa F. HPLC quantification of doxorubicin in plasma and tissues of rats treated with doxorubicin loaded poly(alkylcyanoacrylate) nanoparticles. J Chormatogr B. 2012; 888:128–32.

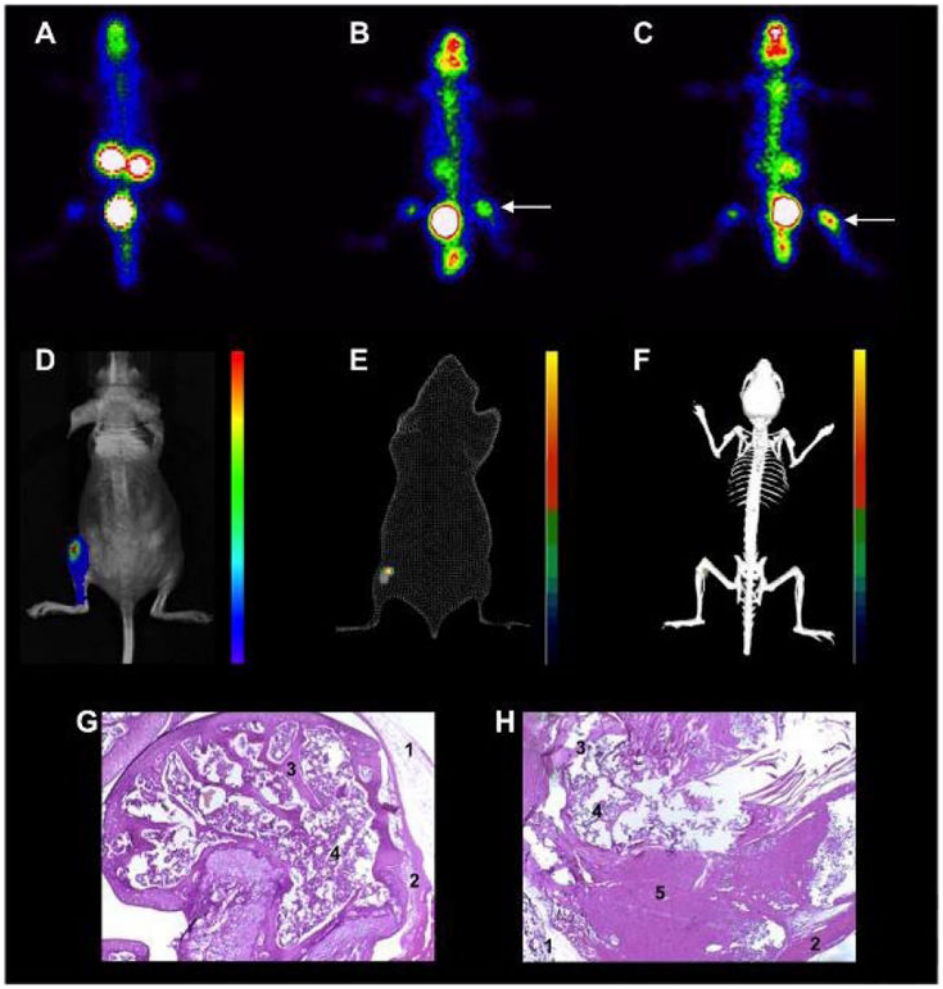

Figure 1.

Representative images of metastatic bone tumor development in mice. Scintigraphic images acquired 1 h post-injection of ^{99m}Tc-MDP of a healthy (A) and a tumor-bearing (B) mouse. The arrow shows the tumor region. Presence of tumor was confirmed by scintigraphic images 1 h post-injection of ^{99m}Tc-BBN$_{7–14}$ (C). Animals were also analyzed by optical imaging (bioluminescence) in bidimensional (D) or tridimensional mode, compared to a body surface (E) or skeletal model (F). Tumor cells were detected in the tibiofemural joint and also spread into the tibial cavity. Histological analysis after of healthy (G) and tumor-bearing tibia (H) using hematoxylin-eosin staining, magnification 10x. We observed intact epithelium (1), muscle (2), bone trabeculae (3) and spongeous bone (4) in healthy tibia, while for the tumor-bearing tibia the trabecular and spongeous bone are reduced being partially replaced by tumor cells (5).

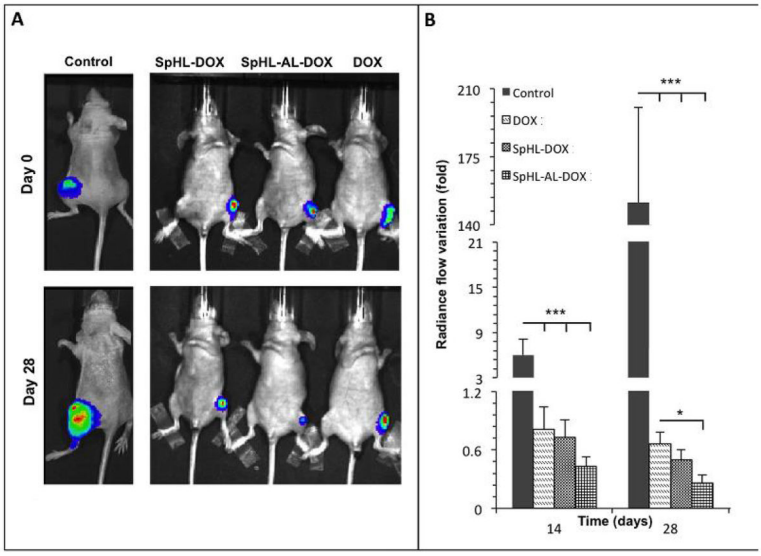

Figure 2.

Representative images of bone tumor-bearing mice prior to and 4 weeks after treatment with free or liposomal DOX at 10 mg•kg^{-1} (A). Quantification of variation in D-luciferin radiance flow into the tumor region compared to the day 0 (B). Results are represented as mean ± standard deviation. Comparison of significant differences between groups at the same time point (* = $p < 0.05$, *** = $p < 0.001$, one-way ANOVA followed by Tukey's test).

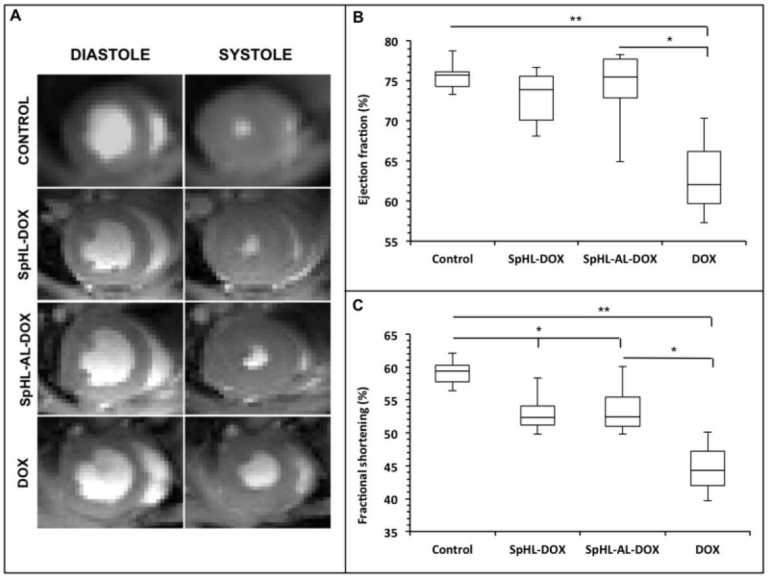

Figure 3.

Representative in vivo MR images of treated animal hearts at the end of diastole (left images) and systole (right images) showing the shortening of left ventricle volume (A). Quantification of ejection fraction (B) and fractional shortening (C) for the animals treated with free or liposomal DOX. Results are expressed as median and inter-quartile range for control (n = 5), SpHL-DOX (n = 5), SpHL-AL-DOX (n = 8), and DOX (n = 3) groups. Comparisons for significant differences between the groups (* = $p < 0.05$, ** = $p < 0.01$) used Kruskall-Wallis' test followed by Dunns' test).

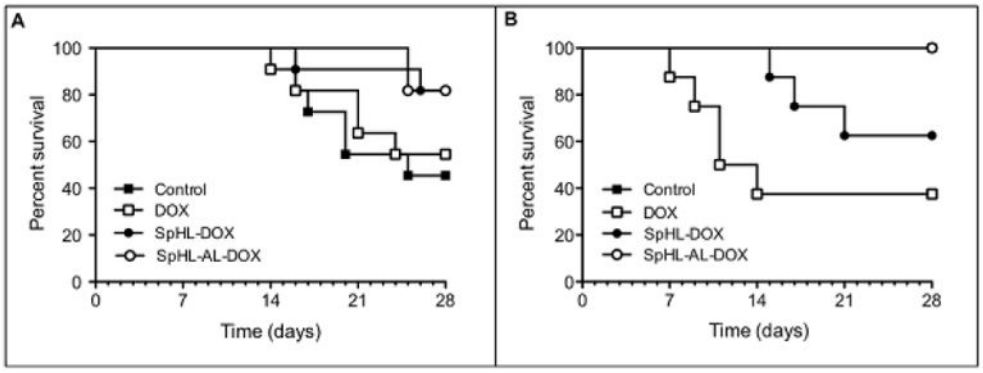

Figure 4.

Kaplan-Meier survival curves for tumor-bearing (A) or healthy (B) mice treated with free or liposomal DOX at 10 mg•kg^{-1}. In B, control (n = 5) and SpHL-AL-DOX (n = 8) survival curves were plotted together because no deaths were observed in these groups throughout the time interval evaluated.

Table 1

Physicochemical parameters for SpHL-DOX and SpHL-AL-DOX*

Formulation	Average diameter (nm)	PdI	Zeta Potential (mV)	Encapsulation Efficacy†
SpHL-DOX	143 ± 11	0.09 ± 0.01	−6.8 ± 1.2	72 ± 3 % 1.4 ± 0.1 mg•mL^{-1}
SpHL-AL-DOX	153 ± 16	0.12 ± 0.02	−15.4 ± 2.3≠	97 ± 2 %≠ 1.9 ± 0.1 mg•mL^{-1}

*Results are represented as mean ± standard deviation (n = 3).

†Encapsulation efficacy is represented as % of doxorubicin encapsulated in the liposomes and final concentration of DOX in the liposomal dispersion (mg•mL^{-1}).

≠indicates statistically significant difference between the SpHL-AL-DOX and SpHL-DOX ($p < 0.05$, t-test).

Table 2

Biodistribution profile (presented as % injected dose•g^{-1} of tissue) of free DOX, SpHL-DOX or SpHL-AL-DOX after 2 or 8 hours post injection in tumor-bearing mice *

Organ	free DOX	SpHL-DOX	SpHL-AL-DOX
		2h	
Liver	1.3 ± 0.4	12.5 ± 3.1†	9.4 ± 1.3†
Spleen	1.2 ± 0.3	11.4 ± 1.1†	7.6 ± 1.4†
Kidney	10.2 ± 2.3†	5.2 ± 1.3†	4.9 ± 1.0†
Heart	1.2 ± 0.4	0.6 ± 0.2	0.4 ± 0.1†
Tumor	0.8 ± 0.3	1.4 ± 0.3	1.7 ± 0.4†
Plasma	0.3 ± 0.1	0.8 ± 0.2†	1.4 ± 0.2†
		8 h	
Liver	-‡	8.3 ± 1.5	5.9 ± 1.0
Spleen	-‡	12.2 ± 2.1	4.2 ± 0.8
Kidney	1.6 ± 0.3	3.1 ± 0.9†	2.1 ± 0.6
Heart	0.1 ± 0.05	-‡	0.1 ± 0.04
Tumor	0.3 ± 0.1	0.5 ± 0.3	1.1 ± 0.2†
Plasma	-‡	0.2 ± 0.1	0.3 ± 0.1

* The results are represented as mean ± standard deviation (n = 3).

† indicates significant difference between the liposomal formulations (SpHL-DOX or SpHL-AL-DOX) compared to free DOX ($p < 0.05$, t-test).

‡ indicates values below the limit of quantification.

Table 3

Mortality parameter analyses of animal treated with free or liposomal DOX

Groups	Survival median (days)	*vs.* control		*vs.* SpHL-AL-DOX	
		p-value	risk ratio	p-value	risk ratio
Healthy animals					
Control	> 28	-	-	1.0000	1.000
SpHL-DOX	> 28	0.1410	5.618	0.0628	8.650
SpHL-AL-DOX	> 28	1.0000	1.000	-	-
DOX	12.5	0.0364	6.944	0.0087	11.236
Tumor bearing animals					
Control	25	-	-	0.0473	4.416
SpHL-DOX	> 28	0.0741	0.269	0.9828	1.022
SpHL-AL-DOX	> 28	0.0473	0.226	-	-
DOX	> 28	0.6516	0.755	0.1125	3.461

Nanomedicine. Author manuscript; available in PMC 2018 July 01.